applied sciences

MDPI

Communication

First Theoretical Realization of a Stable Two-Dimensional Boron Fullerene Network

Bohayra Mortazavi

Department of Mathematics and Physics, Leibniz Universität Hannover, Appelstraße 11, 30167 Hannover, Germany; bohayra.mortazavi@gmail.com

Abstract: Successful experimental realizations of two-dimensional (2D) C_{60} fullerene networks have been among the most exciting latest advances in the rapidly growing field of 2D materials. In this short communication, on the basis of the experimentally synthesized full boron B_{40} fullerene lattice, and by structural minimizations of extensive atomic configurations via density functional theory calculations, we could, for the first time, predict a stable B_{40} fullerene 2D network, which shows an isotropic structure. Acquired results confirm that the herein predicted B_{40} fullerene network is energetically and dynamically stable and also exhibits an appealing thermal stability. The elastic modulus and tensile strength are estimated to be 125 and 7.8 N/m, respectively, revealing strong bonding interactions in the predicted nanoporous nanosheet. Electronic structure calculations reveal metallic character and the possibility of a narrow and direct band gap opening by applying the uniaxial loading. This study introduces the first boron fullerene 2D nanoporous network with an isotropic lattice, remarkable stability, and a bright prospect for the experimental realization.

Keywords: 2D fullerene; boron fullerene; density functional theory; theoretical prediction

Citation: Mortazavi, B. First Theoretical Realization of a Stable Two-Dimensional Boron Fullerene Network. *Appl. Sci.* **2023**, *13*, 1672. https://doi.org/10.3390/app13031672

Academic Editors: Elena Korznikova and Andrey Kistanov

Received: 17 January 2023
Revised: 26 January 2023
Accepted: 27 January 2023
Published: 28 January 2023

1. Introduction

Fullerenes were originally zero-dimensional (0D) carbon-based polyhedral cages consisting of hexagonal and pentagonal rings, which, depending on their number of atoms and topology, can appear in diverse stable forms [1–6]. In 2022, Hou et al. [7] reported the first successful synthesis of a quasi-hexagonal-phase C_{60} fullerene 2D lattice. Shortly after, two other experimental groups also fabricated 2D forms of C_{60} fullerene networks [8,9]. These latest experimental advances [7–9] offer novel fabrication approaches to forming nanoporous and light-weight 2D systems made of 0D fullerene cages connected by 1D bonds with remarkable stability [10–12] and low thermal conductivities [6,10]. It is worth mentioning that after the discovery of C_{60} fullerene [2], it took almost two decades for the experimental realization of the full boron B_{40} fullerene counterpart [13]. On the other side, it also took almost a decade after the experimental realization of the single-layer graphene [14–16] for three different 2D borophene lattices to be first successfully synthesized using epitaxial growth over a silver substrate [17,18]. As an interesting matter of fact, the possibility of the synthesis of borophene nanosheets and their metallic electronic nature were theoretically predicted before their experimental fabrications [19,20].

Boron atoms, similar to their carbon neighbor, show outstanding capabilities to form various bonding architecture, and in 2D form they can appear with buckled or fully planar structures. As it is clear, the recent experimental accomplishments for the synthesis of full carbon 2D fullerene networks [7–9] might be extendable for the case of boron-based counterparts. In fact, B_{40} fullerene can be considered as the basis for the new experimental and theoretical endeavors, taking into account that it is experimentally producible [13] and is already predicted to form bonding interactions with neighboring cages [21]. In this short communication, on the basis of the experimentally fabricated B_{40} boron fullerene, and by the screening of diverse possible 2D configurations, we could successfully predict the

first 2D boron fullerene network. To this aim, we conducted extensive density functional theory (DFT) simulations to perform the energy minimization for detecting the stable atomic configuration and, furthermore, investigated its corresponding bonding, structural, stability, mechanical, and electronic features. The presented DFT results confirm the remarkable energetic, thermal, dynamical, and mechanical stability of the herein predicted isotropic B_{40} fullerene 2D lattice, which makes it highly appealing for further theoretical and experimental endeavors.

2. Computational Methods

DFT calculations herein were carried out using the Vienna ab initio simulation package (VASP) [22,23] on the basis of Perdew–Burke–Ernzerhof (PBE) and generalized gradient approximation (GGA), using DFT-D3 [24] van der Waals (vdW) dispersion correction and cutoff energy of 550 eV for plane waves. With the aforementioned details, in our earlier study [10] the lattice parameters of the experimentally realized 2D C_{60} network were precisely reproduced. In order to conduct the energy minimization, $5 \times 5 \times 1$ Monkhorst–Pack [25] k-point grid was used, until the fulfilment of the energy and force convergence of 10^{-5} eV and 0.001 eV/Å, respectively, with considering a fixed 20 Å for the three-dimensional periodic box size along the thickness. Since the PBE/GGA method methodically underestimates the band gap, HSE06 hybrid functional [26] was also adopted for more accurate investigation of electronic band structure. For the single B_{40} cage, we used $1 \times 1 \times 1$ k-point with the fixed 17 Å box size along the three Cartesian directions. Ab initio molecular dynamics (AIMD) simulations were carried out using the $2 \times 1 \times 1$ supercell and with a fixed time step of 1 fs, in order to inspect the thermal stability. We trained a moment tensor potentials (MTP) [27] with cutoff distance of 3.5 Å to examine the dynamical stability, using AIMD datasets prepared by employing the unit cell structure, DFT-D3 [24] vdW correction, and a $3 \times 3 \times 1$ Monkhorst–Pack K-point grid. The training dataset was prepared by two separate AIMD calculations, for which the systems' temperature was gradually increased from 10 to 100, and from 100 to 2000 K within 1000 time steps (simulation time of 1 ps). The original 2000 AIMD configurations were subsampled, and 830 configurations were used for the fitting of the MTP, which was subsequently used to obtain phonon dispersion relation over the $5 \times 5 \times 1$ supercell, using the PHONOPY package [28], as extensively validated in our earlier study [29].

3. Results and Discussion

We first investigate the structural, bonding, and energetic characteristics of the predicted full boron nanosheet. Figure 1a shows the molecular geometry of the experimentally observed B_{40} cage and its corresponding energy, which was predicted to be -6.079 eV/atom. In order to find the local minimum energy 2D lattice, after the energy minimization of the B_{40} cage, we applied three random rotations along the three Cartesian directions with respect to the center of the atomic mass. After randomly orienting the B_{40} cage, the simulation box size was altered to form primary bonds with periodic images, following by the DFT energy minimization step. By conducting the calculations for around 300 randomly fabricated lattices, we could predict the first minimum energy B_{40}-based 2D network, which is shown in Figure 1b. This novel 2D netwrok presents an isotropic lattice with a length of 7.638 Å, and corresponding energy of -6.230 eV/atom. As the first important finding, the distinctly lower energy of the herein predicted B_{40} fullerene 2D lattice, lower by -0.151 eV/atom compared to the native B_{40} cage, confirms its favorable energetic stability. The lengths of various B-B bonds were found to be close to each other and around 1.75 Å. It should be noted that according to the spin-polarized calculations, it was confirmed that the herein predicted B_{40} fullerene network is not magnetic. In order to examine the bonding mechanism, in Figure 1c the electron localization function (ELF) [30] of the B_{40} fullerene network with an isosurface value of 0.75 is illustrated. ELF is a topological function and varies from 0 to 1. Rather large ELF values over 0.75 around the center of B-B bonds interestingly indicate the covalent nature of interactions in this novel full boron nanosheet.

To facilitate the oncoming studies, atomic structures of the energy minimized 2D and 0D B_{40} lattices are included in the Supporting Information document.

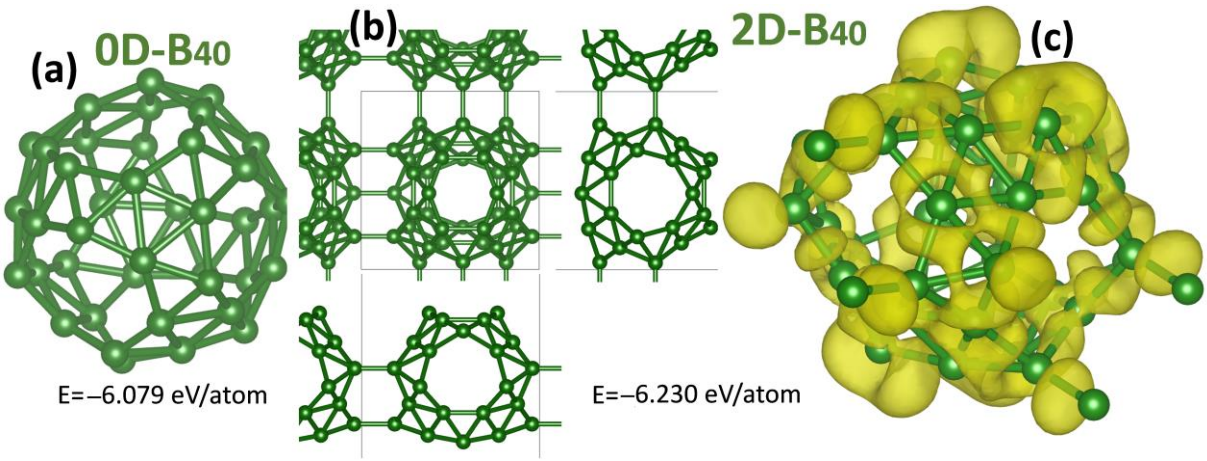

Figure 1. (**a**) 3D view of the B_{40} cage. (**b**) Top and side views for the 2D boron fullerene network. (**c**) 3D view for the electronic localization function (with yellow color) of the 2D boron fullerene network with an isosurface value of 0.75, illustrated using the VESTA package [31]. Find the energy minimized structures in the Supporting Information document.

We next elaborately examined the dynamical, thermal, and mechanical stability of the herein predicted B_{40} fullerene nanosheet [32–36]. The phonon dispersion of the single-layer B_{40} network is depicted in Figure 2a, along with the corresponding phonon group velocities in Figure 2b. It is clearly observable that the three acoustic (find Figure 2a inset) and all optical modes are free of imaginary frequencies, confirming the remarkable dynamical stability of the predicted lattice. Moreover, it can be seen that for the frequencies over 10 THz, the phonon branches appear, generally, with flat dispersions, confirming low group velocities, in agreement with results presented in Figure 3b. Consistent with the phonon dispersion of full carbon fullerene nanosheets [6,10], significant band crossing is visible for the both in-plane acoustic and entire optical phonon modes, revealing short phonon lifetimes for the mainstream heat carriers in the predicted single-layer B_{40} network. The in-plane acoustic modes show the highest group velocity of around 9.7 km/s, which is lower than that of the 11.6 km/s predicted for the 2D C_{36} fullerene [6]. The suppressed group velocity for the phonon modes in the predicted structure suggest its lower lattice thermal conductivity compared to the C_{36} counterpart. The mechanical properties and the corresponding stress–strain curve is shown in Figure 2c. The predicted stress–strain relation is uniaxial, meaning that during the entire deformation process, the B_{40} monolayer is under tension only along the loading and remains acceptably stress-free along the perpendicular direction to the loading. The elastic modulus and tensile strength are predicted to be 125 and 7.8 N/m, respectively, revealing rather strong bonding in the predicted nanoporous B_{40} network, consistent with the previously observed covalent interactions. Based on the DFT results for the uniaxially stressed atomic configurations, we could not detect the clear failure behavior, which can be a clear indication of the higher ductility of the predicted boron fullerene structure than that of the carbon-based counterparts [6,10,11]. It is worth noting that the Poisson's ratio is found to be only 0.009. The thermal stability of the B_{40} network was, moreover, tested by the AIMD simulations at three temperatures of 500, 700, and 1000 K for 20 ps long calculations. The AIMD results for the evolution of the per atom total energy for different temperatures are illustrated in Figure 2d, along with the side views for the final atomic configurations. It is observable that up to a moderately high temperature of 700 K, the single-layer B_{40} network stays completely stable, whereas at 1000 K, the lattice is partially distorted. The presented DT results clearly confirm the

outstanding energetic, thermal, dynamical, and mechanical stability of the herein predicted B_{40} fullerene.

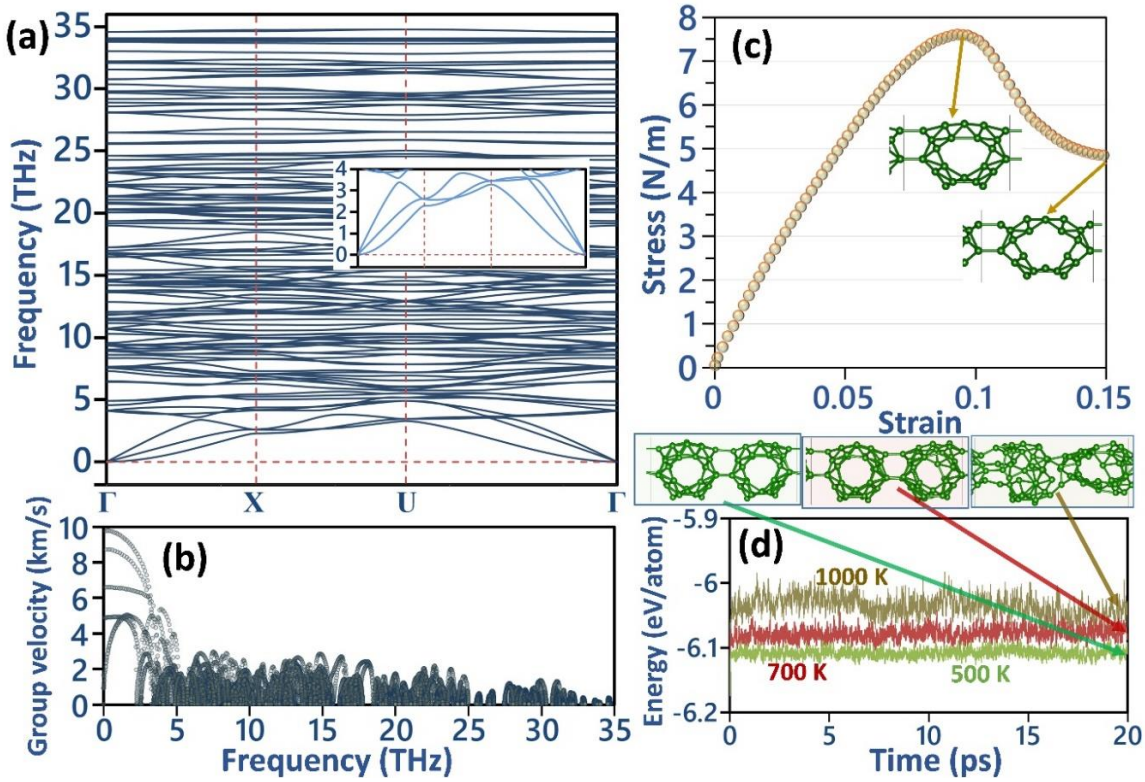

Figure 2. (**a**) Phonon dispersion and (**b**) group velocity of the predicted single-layer B_{40} network. (**c**) Uniaxial stress–strain at the ground state along with side views of the deformed structures. (**d**) The AIMD results for the per atom total energy of the B_{40} nanosheet during the simulations at temperatures of 500, 700, and 1000 K. The insets in panel (**d**) show the side views for the final atomic configurations after 20 ps of AIMD simulations.

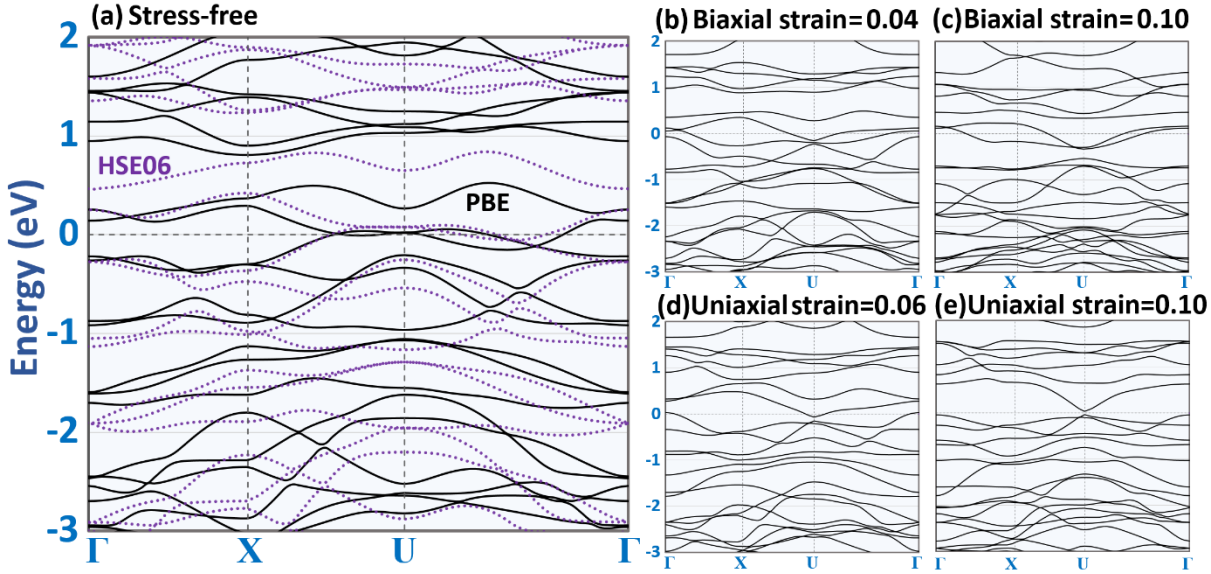

Figure 3. Electronic band structures of the stress-free and strained B_{40} 2D network by the PBE (solid lines) and HSE06 (dotted lines) methods.

Last, but not least, we briefly investigated the electronic character of the predicted B_{40} fullerene 2D network. From the results shown in Figure 3a for the stress-free fullerene network, the metallic electronic character is confirmed by the both considered methods of PBE and HSE06, consistent with those of pristine borophene monolayers. As shown in Figure 3b,c, we found that by applying the biaxial straining, the states around the Fermi level become denser and, consequently, enhance the metallicity of the system. On the other side, by applying the uniaxial loading, the valance and conduction bands around the Fermi energy start to separate, and, as shown in Figure 3e, for a relatively large strain of 0.1, a narrow and direct band gap of 0.07 appears in the electronic structure. These results confirm that the electronic structure of the unstrained and strained B_{40} fullerene monolayers mostly show a metallic nature, with a low possibility of yielding a narrow gap semiconducting character under large uniaxial loading.

4. Concluding Remarks

In this short communication, by performing extensive DFT calculations, we could, for the first time, predict a stable B_{40} boron fullerene nanosheet. The predicted novel full boron 2D lattice shows an isotropic structure with noticeable contribution of covalent interactions, and, excitingly, is energetically more stable than the experimentally available B_{40} fullerene. The B_{40} fullerene 2D network is also confirmed to be dynamically stable, and exhibits thermal stability at a moderately high temperature of 700 K. The elastic modulus, Poisson's ratio, and tensile strength of the predicted 2D lattice are estimated to be 125 N/m, 0.009, and 7.8 N/m, respectively. The unstrained and strained B_{40} fullerene networks mostly show metallic electronic natures, with the possibility of evolving to a narrow and direct gap semiconducting character under the uniaxial loading. This study introduces the first boron fullerene 2D lattice on the basis of the already experimentally available B_{40} fullerene, which shows an isotropic lattice, remarkable stability and strength, and metallic electronic nature, with a bright prospect for experimental synthesis, being highly appealing for further theoretical and experimental endeavors.

Supplementary Materials: The following supporting information can be downloaded at: https://www.mdpi.com/article/10.3390/app13031672/s1, Supporting information: First theoretical realization of a stable two-dimensional boron fullerene network.

Funding: This research was funded by Deutsche Forschungsgemeinschaft (DFG, German Research Foundation) under Germany's Excellence Strategy within the Cluster of Excellence PhoenixD (EXC 2122, Project ID 390833453).

Institutional Review Board Statement: Not applicable.

Informed Consent Statement: Not applicable.

Data Availability Statement: Atomic structures of the energy-minimized 2D and 0D B40 lattices are included in the Supporting Information document. Additional data presented in this study are also available on request from the corresponding author.

Acknowledgments: The author is greatly thankful to the VEGAS cluster team at Bauhaus University of Weimar for providing the computational resources.

Conflicts of Interest: The author has no conflict of interest to declare that are relevant to the content of this article.

References

1. Schwerdtfeger, P.; Wirz, L.N.; Avery, J. The topology of fullerenes. *WIREs Comput. Mol. Sci.* **2015**, *5*, 96–145. [CrossRef] [PubMed]
2. Ge, M.; Sattler, K. Observation of fullerene cones. *Chem. Phys. Lett.* **1994**, *220*, 192–196. [CrossRef]
3. Schwerdtfeger, P.; Wirz, L.; Avery, J. Program Fullerene: A software package for constructing and analyzing structures of regular fullerenes. *J. Comput. Chem.* **2013**, *34*, 1508–1526. [CrossRef] [PubMed]
4. Shakirova, A.A.; Tomilin, F.N.; Pomogaev, V.A.; Vnukova, N.G.; Churilov, G.N.; Kudryasheva, N.S.; Tchaikovskaya, O.N.; Ovchinnikov, S.G.; Avramov, P. Synthesis, Mass Spectroscopy Detection, and Density Functional Theory Investigations of the Gd Endohedral Complexes of C82 Fullerenols. *Computation* **2021**, *9*, 58. [CrossRef]

5. Melchakova, I.A.; Tenev, T.G.; Vitanov, N.V.; Tchaikovskaya, O.N.; Chernozatonskii, L.A.; Yakobson, B.I.; Avramov, P.V. Extreme structure and spontaneous lift of spin degeneracy in doped perforated bilayer graphenes. *Carbon* **2022**, *192*, 61–70. [CrossRef]
6. Mortazavi, B.; Shojaei, F.; Zhuang, X. A novel two-dimensional C36 fullerene network; an isotropic, auxetic semiconductor with low thermal conductivity and remarkable stiffness. *Mater. Today Nano* **2023**, *21*, 100280. [CrossRef]
7. Hou, L.; Cui, X.; Guan, B.; Wang, S.; Li, R.; Liu, Y.; Zhu, D.; Zheng, J. Synthesis of a monolayer fullerene network. *Nature* **2022**, *606*, 507–510. [CrossRef]
8. Pan, F.; Ni, K.; Xu, T.; Chen, H.; Wang, Y.; Gong, K.; Liu, C.; Li, X.; Lin, M.-L.; Li, S.; et al. Long-range ordered porous carbons produced from C60. *Nature* **2023**, 1–7. [CrossRef]
9. Meirzadeh, E.; Evans, A.M.; Rezaee, M.; Milich, M.; Dionne, C.J.; Darlington, T.P.; Bao, S.T.; Bartholomew, A.K.; Handa, T.; Rizzo, D.J.; et al. A few-layer covalent network of fullerenes. *Nature* **2023**, *613*, 71–76. [CrossRef]
10. Mortazavi, B.; Zhuang, X. Low and Anisotropic Tensile Strength and Thermal Conductivity in the Single-Layer Fullerene Network Predicted by Machine-Learning Interatomic Potentials. *Coatings* **2022**, *12*, 1171. [CrossRef]
11. Ying, P.; Dong, H.; Liang, T.; Fan, Z.; Zhong, Z.; Zhang, J. Atomistic insights into the mechanical anisotropy and fragility of monolayer fullerene networks using quantum mechanical calculations and machine-learning molecular dynamics simulations. *Extrem. Mech. Lett.* **2023**, *58*, 101929. [CrossRef]
12. Shen, G.; Li, L.; Tang, S.; Jin, J.; Chen, X.; Peng, Q. Stability and Elasticity of Quasi-Hexagonal Fullerene Monolayer from First-Principles Study. *Crystals* **2023**, *13*, 224. [CrossRef]
13. Zhai, H.-J.; Zhao, Y.-F.; Li, W.-L.; Chen, Q.; Bai, H.; Hu, H.-S.; Piazza, Z.; Tian, W.-J.; Lu, H.-G.; Wu, Y.-B.; et al. Observation of an all-boron fullerene. *Nat. Chem.* **2014**, *6*, 727–731. [CrossRef]
14. Geim, A.K.; Novoselov, K.S. The rise of graphene. *Nat. Mater.* **2007**, *6*, 183–191. [CrossRef]
15. Neto, A.H.C.; Peres, N.M.R.; Novoselov, K.S.; Geim, A.K.; Guinea, F. The electronic properties of graphene. *Rev. Mod. Phys.* **2009**, *81*, 109–162. [CrossRef]
16. Novoselov, K.S.; Geim, A.K.; Morozov, S.V.; Jiang, D.; Zhang, Y.; Dubonos, S.V.; Grigorieva, I.V.; Firsov, A.A. Electric field effect in atomically thin carbon films. *Science* **2004**, *306*, 666–669. [CrossRef]
17. Mannix, A.J.; Zhou, X.-F.; Kiraly, B.; Wood, J.D.; Alducin, D.; Myers, B.D.; Liu, X.; Fisher, B.L.; Santiago, U.; Guest, J.R.; et al. Synthesis of borophenes: Anisotropic, two-dimensional boron polymorphs. *Science* **2015**, *350*, 1513–1516. [CrossRef]
18. Feng, B.; Zhang, J.; Zhong, Q.; Li, W.; Li, S.; Li, H.; Cheng, P.; Meng, S.; Chen, L.; Wu, K. Experimental Realization of Two-Dimensional Boron Sheets. *Nat. Chem.* **2016**, *8*, 563–568. [CrossRef]
19. Zhou, X.F.; Dong, X.; Oganov, A.R.; Zhu, Q.; Tian, Y.; Wang, H.T. Semimetallic two-dimensional boron allotrope with massless Dirac fermions. *Phys. Rev. Lett.* **2014**, *112*, 085502. [CrossRef]
20. Zhang, Z.; Yang, Y.; Gao, G.; Yakobson, B.I. Two-Dimensional Boron Monolayers Mediated by Metal Substrates. *Angew. Chemie* **2015**, *127*, 13214–13218. [CrossRef]
21. Yang, L.; Li, Y.; Hao, D.; Li, L.; Peng, H.; Jin, P. Aggregation behavior and non-covalent functionalization of borofullerenes B28, B38, and B40: A density functional theory investigation. *Int. J. Quantum Chem.* **2019**, *119*, e25921. [CrossRef]
22. Kresse, G.; Furthmüller, J. Efficient iterative schemes for ab initio total-energy calculations using a plane-wave basis set. *Phys. Rev. B* **1996**, *54*, 11169–11186. [CrossRef] [PubMed]
23. Perdew, J.P.; Burke, K.; Ernzerhof, M. Generalized Gradient Approximation Made Simple. *Phys. Rev. Lett.* **1996**, *77*, 3865–3868. [CrossRef] [PubMed]
24. Grimme, S.; Antony, J.; Ehrlich, S.; Krieg, H. A consistent and accurate ab initio parametrization of density functional dispersion correction (DFT-D) for the 94 elements H-Pu. *J. Chem. Phys.* **2010**, *132*, 154104. [CrossRef] [PubMed]
25. Monkhorst, H.; Pack, J. Special points for Brillouin zone integrations. *Phys. Rev. B* **1976**, *13*, 5188–5192. [CrossRef]
26. Krukau, A.V.; Vydrov, O.A.; Izmaylov, A.F.; Scuseria, G.E. Influence of the exchange screening parameter on the performance of screened hybrid functionals. *J. Chem. Phys.* **2006**, *125*, 224106. [CrossRef]
27. Shapeev, A.V. Moment tensor potentials: A class of systematically improvable interatomic potentials. *Multiscale Model. Simul.* **2016**, *14*, 1153–1173. [CrossRef]
28. Togo, A.; Tanaka, I. First principles phonon calculations in materials science. *Scr. Mater.* **2015**, *108*, 1–5. [CrossRef]
29. Mortazavi, B.; Novikov, I.S.; Podryabinkin, E.V.; Roche, S.; Rabczuk, T.; Shapeev, A.V.; Zhuang, X. Exploring phononic properties of two-dimensional materials using machine learning interatomic potentials. *Appl. Mater. Today* **2020**, *20*, 100685. [CrossRef]
30. Silvi, B.; Savin, A. Classification of Chemical-Bonds Based on Topological Analysis of Electron Localization Functions. *Nature* **1994**, *371*, 683–686. [CrossRef]
31. Momma, K.; Izumi, F. VESTA 3 for three-dimensional visualization of crystal, volumetric and morphology data. *J. Appl. Crystallogr.* **2011**, *44*, 1272–1276. [CrossRef]
32. Gardeh, M.G.; Kistanov, A.A.; Nguyen, H.; Manzano, H.; Cao, W.; Kinnunen, P. Exploring Mechanisms of Hydration and Carbonation of MgO and Mg(OH)2 in Reactive Magnesium Oxide-Based Cements. *J. Phys. Chem. C* **2022**, *126*, 6196–6206. [CrossRef]
33. Kistanov, A.A.; Rani, E.; Singh, H.; Fabritius, T.; Huttula, M.; Cao, W. Discerning phase-matrices for individual nitride inclusions within ultra-high-strength steel: Experiment driven DFT investigation. *Phys. Chem. Chem. Phys.* **2022**, *24*, 1456–1461. [CrossRef]
34. Kistanov, A.A.; Shcherbinin, S.A.; Botella, R.; Davletshin, A.; Cao, W. Family of Two-Dimensional Transition Metal Dichlorides: Fundamental Properties, Structural Defects, and Environmental Stability. *J. Phys. Chem. Lett.* **2022**, *13*, 2165–2172. [CrossRef]

35. Arabha, S.; Rajabpour, A. Thermo-mechanical properties of nitrogenated holey graphene (C2N): A comparison of machine-learning-based and classical interatomic potentials. *Int. J. Heat Mass Transf.* **2021**, *178*, 121589. [CrossRef]
36. Arabha, S.; Aghbolagh, Z.S.; Ghorbani, K.; Hatam-Lee, M.; Rajabpour, A. Recent advances in lattice thermal conductivity calculation using machine-learning interatomic potentials. *J. Appl. Phys.* **2021**, *130*, 210903. [CrossRef]